International Journal of Fatigue 104 (2017) 322–333

Contents lists available at ScienceDirect

International Journal of Fatigue

journal homepage: www.elsevier.com/locate/ijfatigue

Statistical size effect on multiaxial fatigue strength of notched steel components

Martin Leitner [a,*], Michael Vormwald [b], Heikki Remes [c]

[a] Montanuniversität Leoben, Chair of Mechanical Engineering, Leoben, Austria
[b] Technische Universität Darmstadt, Materials Mechanics Group, Darmstadt, Germany
[c] Aalto University, Department of Mechanical Engineering, Espoo, Finland

ARTICLE INFO

Article history:
Received 7 June 2017
Received in revised form 1 August 2017
Accepted 2 August 2017
Available online 3 August 2017

Keywords:
Fatigue strength
Notched components
Multiaxial loading
Statistical size effect
Highly-stressed surface and volume

ABSTRACT

Fatigue strength assessment of large-scale structures and components is usually performed on the basis of experimental results from small-scale specimens. A proper transfer from small specimens to large-scale structures requires the consideration of size and stress-gradient induced micro supports effects, which depend on material to loading type. This paper investigates statistical size effects on the fatigue strength of notched electroslag remelted 50CrMo4 steel components under uniaxial and multiaxial loadings. Firstly, stress-based micro support concepts utilizing uniaxial small-scale tests are applied to enable an accurate fatigue design of notched steel parts. Then, the notched large-scale specimens, as representatives for an engineering component, are tested under uniaxial transverse and rotating bending as well as multiaxial loading for validation purpose. Secondly, stress-based methods with highly-stressed surface area and volume are applied in order to consider the fatigue support and statistical size effects. The estimated fatigue strength at the high-cycle regime shows a sound conformity to the large-scale experiments with a maximum deviation of 7.4% in case of the surface, and of 4.3% by the volume approach. The results of the present investigation also reveal that a certain upper threshold value is required for the highly-stressed volume concept in advance in order to ensure a proper fatigue strength assessment. The threshold value is not required for the surface approach and thus, it is found to be more feasible to an engineering purpose, especially in case of surface-initiated fatigue failure modes.

1. Introduction

Generally, it is well known that size effects may have significant influence on the fatigue strength of engineering materials and components [1]. Numerous studies for steel [2], cast iron [3], aluminium [4] as well as other materials [5,6] and manufacturing as well as loading conditions [7–9] validate the existence of such fatigue size effects in a wide field of application. In accordance to [10], the general term size effect can be distinguished in

- the statistical size effect [11–13]
- the geometrical size effect [14–16],
- the technological size effect [17–19], and
- the surface-technological size effect, e.g. for surface hardened parts [20].

This paper focuses on the investigation of the statistical size effect for notched 50CrMo4 steel components under multiaxial proportional load conditions. Therefore, not only the statistical aspect has to be considered, but additionally the geometrical fatigue support effect at the root of the notch needs to be taken into account [21]. Within the design process, these two influences are usually incorporated on the basis of a fatigue support number n, see Eq. (1), which is also implemented in commonly applied design recommendations, such as the FKM-guideline [22]. A detailed summary of the FKM-guideline is provided in [23].

$$n = \frac{K_t}{K_f} \tag{1}$$

Herein, K_t equals the stress concentration factor as ratio between the local stress at the notch root and the nominal stress of the adjacent cross-section, and K_f is known as the fatigue factor defined by the nominal high-cycle fatigue strength ratio of the unnotched specimen to the notched component. As a complex component does not facilitate a proper definition of a nominal cross-section, the application of notch stress-based concepts [24] is widespread

* Corresponding author.
E-mail address: martin.leitner@unileoben.ac.at (M. Leitner).

http://dx.doi.org/10.1016/j.ijfatigue.2017.08.002
0142-1123/

Nomenclature

A	highly-stressed surface area
AB	axial (transverse) bending loading
a	exponent of model n_{II}
$\hat{a}$	material parameter of model $n_{I,FM}$
a^*	material parameter of model $n_{I,FM}$
a_G	material parameter of model $n_{I,SG}$
b_G	material parameter of model $n_{I,SG}$
d	specimen diameter
E	Young's modulus
ESR	electro slag remelting
f_u	ultimate strength
$f_{u,ref}$	reference ultimate strength
K_D	parameter of model $n_{II,SG}$
K_f	fatigue notch factor
K_t	stress concentration factor
k	slope in finite life region/Weibull parameter
N	number of load-cycles to failure
n	fatigue support number
n′	parameter of model $n_{I,MS}$
R	stress ratio or Notch radius
RB	rotating bending loading
s_g	material-dependent length of sliding layer
T/C	tension/compression loading
V	highly-stressed volume
χ'	relative stress gradient at notch
ρ^*	microstructural support length
σ	normal stress
$\bar{\sigma}$	average normal stress
σ_0	far-field tensile loading
σ_{max}	maximum stress at notch root
σ_R	normal fatigue resistance
τ	shear stress

within numerical design processes. Thereby, the notch fatigue resistance σ_R under fully reversed load stress can be determined incorporating the fatigue strength of the unnotched specimen under alternating tension/compression (T/C) loading $\sigma_{T/C,R}$ and the fatigue support number n on basis of Eq. (2).

$$\sigma_R = \sigma_{T/C,R} \cdot n \tag{2}$$

The geometrical fatigue support effect for notched components is usually called as micro support effect and it is commonly taken into account by the relative stress gradient χ' at the surface of the notch root [25]. This value is calculated by Eq. (3), at which the linear-elastic stress distribution $\sigma(x)$ in surface normal depth x or perpendicular to maximum principal stress at the point of the highest notch stress σ_{max} is utilized.

$$\chi' = \frac{1}{\sigma_{max}} \cdot \left| \frac{d\sigma(x)}{dx} \right| \tag{3}$$

Based on the principle of this stress gradient definition, the effective stress for the fatigue assessment can be derived by an averaging of the local surface-near stress distribution over a certain length. In addition, reference distance or volume based approaches are proposed. An overview of common approaches and their general theory is provided in [26].

Among them, the stress averaging concept by Neuber [27] acts as one fundamental method, which is also applied for sharp notched components considering the microstructural support effect [28]. Herein, the average stress $\bar{\sigma}$ at the notch root area is evaluated by an averaging of the stress distribution in depth $\sigma(x)$ over a material dependent microstructural support length ρ^*, see Eq. (4).

$$\bar{\sigma} = \frac{1}{\rho^*} \cdot \int_0^{\rho^*} \sigma(x) dx \tag{4}$$

Further on, the fatigue support number n is calculated by Eq. (5) assuming a local stress distribution computed for a notch under a far-field tensile loading σ_0 according to [29].

$$n = \frac{\sigma_0}{\bar{\sigma}} = \sqrt{1 + \rho^* \cdot \chi'} \tag{5}$$

Similar methods on the basis of the introduced stress averaging approach are presented by Peterson [30] and Heywood [31], whereby a review of these concepts is given in [32]. Siebel and Stieler [33] suggest another empirical stress gradient based approach, where s_g defines a characteristic material-dependent length, which basically acts as indicator of the sliding layer in the course of plastic deformation at the notch, see Eq. (6) [34]. Due to its engineering-feasible applicability, this method serves as fundament for several fatigue design guidelines, such as presented by [22,35,36].

$$n = 1 + \sqrt{s_g \cdot \chi'} \tag{6}$$

On the contrary to the aforementioned stress gradient concepts taking a characteristic material length into account, the empirical approach by Eichlseder [37] utilizes the experimentally evaluated fatigue strength under fully reversed tension/compression $\sigma_{T/C,R}$ and bending loading $\sigma_{B,R}$ for an unnotched specimen under an alternating stress ratio. This industrial-practicable procedure is implemented in a common finite element post-processor tool for fatigue strength analyses of multiaxially loaded components [38] and several applications, see [33,22,37].

Besides the influence due to the stress gradient, an additional enhancement of the fatigue assessment by the statistical size effect increases its accuracy and therefore, majorly improves the fatigue life evaluation within the design process. Surface or volume dependent parameters [39] commonly act as basis for a probabilistic fatigue assessment using Weibull's statistical theory of the strength of materials [40]. A study in [41], on the basis of preliminary experiments in [42], reveals the applicability of this concept, whereby the relationship of the fatigue resistance σ_R between two unnotched specimens of different sizes depends on their highly-stressed surface areas A utilizing the Weibull parameter k, see Eq. (7).

$$\frac{\sigma_{R,1}}{\sigma_{R,2}} = \left(\frac{A_2}{A_1} \right)^{\frac{1}{k}} \tag{7}$$

A subsequent investigation in [43] facilitates this approach in order to assess statistical as well as geometrical size effects in notched members based on weakest-link and short-crack modelling. The presented procedure is additionally included in the recent edition of the FKM-guideline [22]. Alternatively to the surface, also the highly-stressed volume may act as relevant parameter to evaluate statistical size effects [44,45]. Considering the introduced stress gradient model by [37], an extension of this method by the highly-stressed volume as main parameter to incorporate statistical size effects within the local fatigue assessment is presented in [46]. A comparison of the results with therein conducted experiments indicates sound conformity and validates the

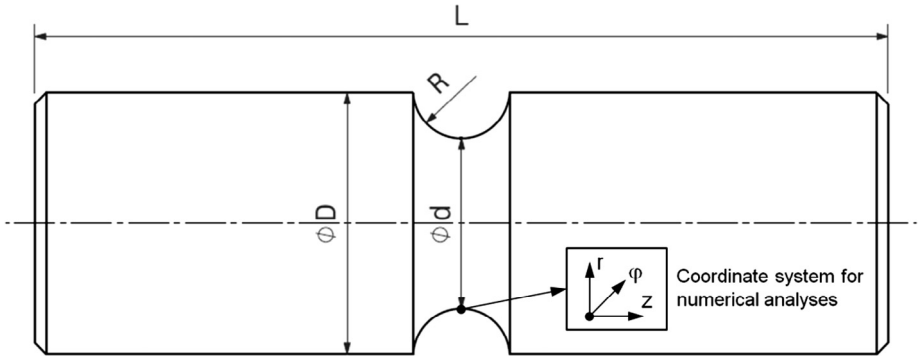

Fig. 1. Geometry of large-scale specimen.

applicability of this suggested concept. However, most of the presented methods are mainly validated for uniaxial loadings, e.g. shown in [47] for different material types under constant amplitude loading, or in [48] for aluminium specimens under variable amplitude load-histories. In case of multiaxial load scenarios, the application of micro support and statistical size effect models needs to be additionally validated. Even though numerous concepts considering the stress gradient and the statistical size effect within the fatigue assessment are available, just some of them incorporate both influences in a combined manner as shown in [22,49–51]. Furthermore, the applicability of such models is mainly validated for uniaxial load conditions and not sufficiently performed for multiaxial load scenarios. Hence, this paper contributes to improve the fatigue strength assessment of notched steel components considering both micro support and statistical size effects under multiaxial load conditions.

The investigations shown in this paper cover both experimental and numerical investigations. Firstly, the notch stress analyses of the specimens are performed to define stress gradient effect and highly-stressed surface areas and volumes for different loading types and specimen sizes. Then, the fatigue tests of small and large-scale specimens under uniaxial and multiaxial proportional loading are carried out. The present investigation is focused on two most promising approaches; the surface [43] and volume-based [46] approach to considering both fatigue support and statistical size effects. Based on the validation, which compares the methods with experimental results, the suitability and limitation of these approaches are discussed.

Table 1
Nominal chemical composition of 50CrMo4 steel [54]

C	Si	Mn	Cr	Mo
0.46–0.54	max. 0.40	0.50–0.80	0.90–1.20	0.15–0.30

2. Material and testing methodology

In this work, 50CrMo4 steel is investigated, whereby preliminary fatigue tests for this material type are in-depth presented in [52,53]. Ref. [52] provides detailed information about geometries, manufacturing conditions, and test results of the small-scale specimens, while Ref. [53] shows rotating bending fatigue tests of the large-scale specimens and its manufacturing procedure. To cover varied loading types, this study also carries out additional fatigue tests using the large-scale specimens, see Fig. 1. The testing diameter in the notched region exhibits a value of $d = 30$ mm. Further details regarding the design of the large-scale specimen is provided in [53]. The specified nominal chemical composition of the 50CrMo4 steel according to [54] is presented in Table 1.

The supplementary fatigue experiments are performed under axial (transverse) bending (AB) as well as multiaxial (MA) proportional axial bending and torsion loading. In addition, the results from rotating bending (RB) loading are incorporated, which are specifically presented in [53]. The test set-up for the conducted fatigue testing under AB and MA loading is depicted in Fig. 2. Herein, the alternating cyclic load is applied by a hydraulic cylinder and testing is performed at a frequency of around 10 Hz. The abort criterion is set as burst fracture or at a defined run-out level of five million load-cycles for all investigated test series.

A representation of the specified nominal mechanical properties of 50CrMo4 steel round bars for diameters between 16 mm and 40 mm according to [54] is provided in Table 2.

As mentioned in [52], quasi-static tensile tests reveal sound accordance to the specified mechanical properties and no distinctive effect by the electroslag remelting (ESR), as post-treatment process within the steel manufacturing routine, is observed. Hence, the suggested values in [54] are generally applicable for the investigated large-scale specimens in this work. Due to technological, manufacturing dependent size effects, the yield strength shows a

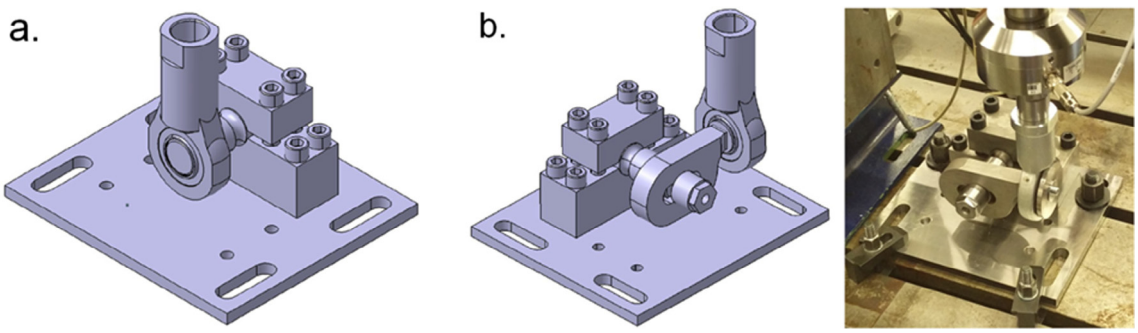

Fig. 2. Test set-up for AB (a) and MA (b) fatigue testing [55].

Table 2
Nominal mechanical properties of 50CrMo4 steel [54]

Yield strength [MPa]	Ultimate strength [MPa]	Elongation at rupture [%]	Reduction of area [%]
780	1000–1200	10	45

specified increase of about 15%, and the ultimate strength of about 10% for the small-scale compared to the large-scale specimens, whereby further details are given in [54].

3. Results of numerical analyses and fatigue tests

This section firstly, shows the results of the numerical analysis for the large-scale specimens, and secondly, summarizes the previously examined findings utilizing the small-scale specimens in [52] and presents the new test results for the large-scale specimens.

3.1. Notch stress and stress-gradient analyses

In order to evaluate the stress condition at the surface and within the volume at the highly-stressed notch region, linear-elastic numerical analyses are performed with the investigated large-scale specimen utilizing hexahedral elements with quadratic shape functions. Similar analyzes are performed for the small-scale specimens [52] to ensure a proper comparability and transfer of the results. The finite element computation result of the large-scale specimen under AB and RB loading is illustrated in Fig. 3. The maximum principal stress plot is depicted for a certain moment during testing, whereby the stress condition is equal for both loading conditions. The results are normalized with an analytically calculated nominal stress in the testing cross-section leading to a maximum principal stress concentration factor of $K_t = 1.43$ at the position of maximum stress σ_{max} at the surface of the notch root.

Based on this surface point, the numerically evaluated stress distribution in depth and in both directions on the surface are pictured in case of AB loading in Fig. 4. Thereby, the stress path is normalized by the notch radius and the corresponding coordinate system at the notch root is presented in Fig. 1, whereby r-direction is oriented radial in depth, z- in axial direction, and φ- in circumferential direction of the specimen. The distribution in r- and z-direction is equal in case of RB loading, but the one in φ-direction arises as constant value exhibiting the maximum stress σ_{max} at every point around the circumference during rotation of the specimen. Hence, the stress gradient in depth is equal between AB and RB loading, but the amount of highly-stressed surface area or volume is majorly different for both conditions.

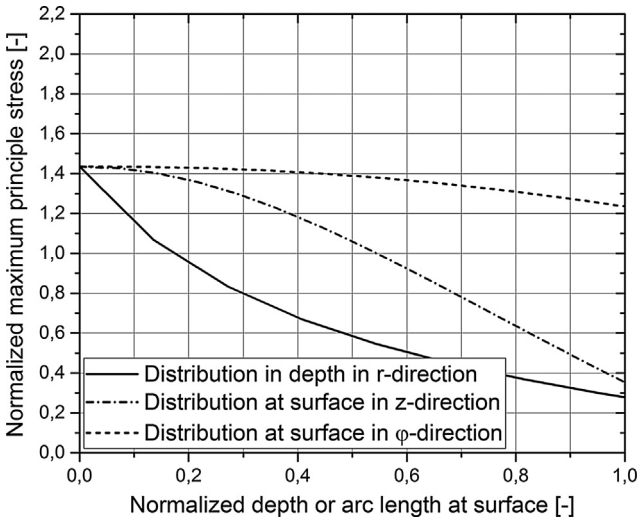

Fig. 4. Maximum principal stress distributions of large-scale specimen under AB loading.

The same numerical analysis is performed for the large-scale specimen under MA loading, see Fig. 5. The multiaxial load stress condition is proportional featuring a similar τ/σ-ratio of about $\tau/\sigma = 0.5$ as applied for the small-scale specimens. Due to the additional shear stress loading an increase of the maximum principal stress concentration factor up to a value of $K_t = 2.12$ compared to the nominal stress under bending loading is observed. Again, the stress distributions in depth and in both surface directions starting from the maximum surface stress point σ_{max} are depicted in Fig. 6.

Generally, similar tendencies are observed in the MA loading as for the uniaxial AB loading case. However, the exact shapes of the distributions in depth and at the surface directions show explicit differences.

3.2. Small-scale specimen tests

As aforementioned, extensive fatigue tests with small-scale specimens including varying notch geometries and loading conditions are executed, see [52]. The tests cover unnotched, mild-notched and sharp-notched specimen geometries at an alternating stress ratio of $R = -1$. The loading types are tension-compression (T/C) and rotation-bending (RB). A statistical evaluation of the fatigue test results based on the ASTM-procedure given in [56] for the finite life region and by the arcsine$_\sqrt{}$P-method introduced in [57] for the high-cycle fatigue regime is conducted. Table 3 summarizes the fatigue test results, which are normalized with respect to the fatigue resistance at five million load-cycles of the unnotched spec-

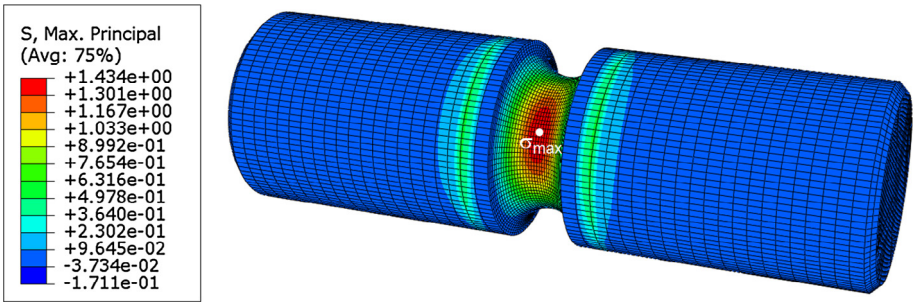

Fig. 3. Result of linear-elastic numerical analysis of large-scale specimen under AB and RB loading.

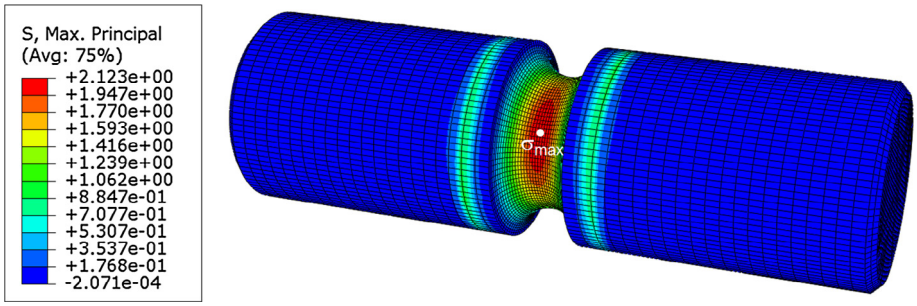

Fig. 5. Result of linear-elastic numerical analysis of large-scale specimen under MA loading.

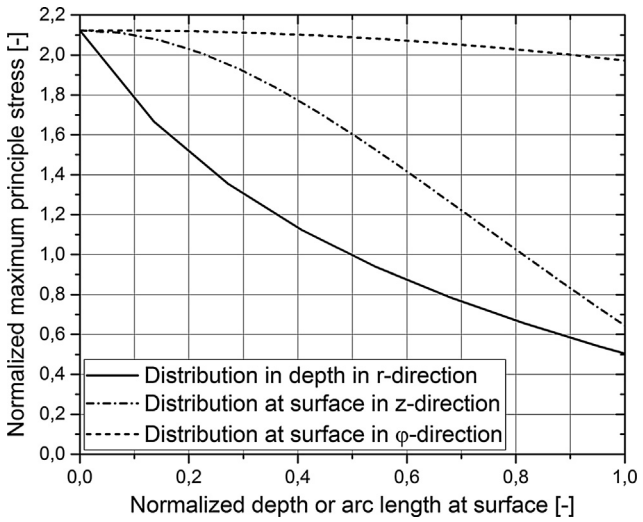

Fig. 6. Maximum principal stress distributions of large-scale specimen under MA loading.

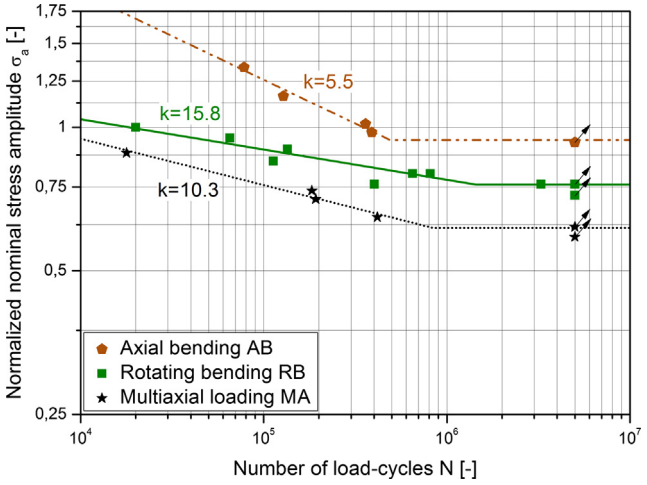

Fig. 7. Nominal fatigue test results for large-scale specimens.

imen under T/C loading. In addition, the corresponding maximum principal stress concentration factor K_t as well as normalized relative stress gradient χ' is shown for each specimen and loading type.

The results clearly indicate that the high-cycle fatigue strength is reduced by increasing the stress concentration factor K_t at the notch root. However, the effect is not as detrimental as a calculation based on K_t would estimate, which validates that a certain micro support effect during fatigue loading occurs. Thus, the consideration of the relative stress gradient χ' is also needed. In addition to the experiments under uniaxial loading shown in Table 3, multiaxial proportional fatigue tests (MA) including normal rotating bending stress σ and shear torsion stress τ at a ratio of $\tau/\sigma = 0.5$ are executed for the unnotched small-scale specimen geometry in [52]. Thereby, the statistically evaluated normal fatigue strength shows a normalized value of $\sigma_R = 0.7$ under this multiaxial stress condition. An application of the multiaxial fatigue model by Gough and Pollard [58] reveals a sound agreement with a minor underestimation of the multiaxial fatigue strength by about 5%, which basically validates the applicability of this commonly utilized hypothesis for the investigated base material. Further details in regard to the experimental results and multiaxial fatigue assessment are provided in [52].

3.3. Large-scale specimen tests

The fatigue test results of the large-scale specimens are depicted in Fig. 7. Thereby, the experiments are performed under axial bending (AB) and rotating bending (RB) as well as multiaxial loading (MA). To ensure a plain comparison to the small-scale specimen fatigue values, the presented results are again normalized with the high-cycle fatigue strength at $N = 5 \cdot 10^6$ load-cycles of the unnotched small-scale specimen under T/C loading. The statistically evaluated fatigue resistance at the run-out level reveals that a decrease of almost 20% occurs from the behaviour under AB to RB loading.

As both these tests have the same geometry and bending loading mode, the stress concentration and relative stress gradient are equal. Therefore, these results clearly indicate a reduction in fatigue strength, which cannot be assessed only based on the micro

Table 3
Summary of uniaxial fatigue test results for small-scale specimens [52]

Loading and specimen type	Normalized nominal fatigue strength	Stress concentration factor K_t	Normalized relative stress gradient χ'
T/C unnotched	1.00	1.00	0.00
RB unnotched	1.10	1.00	0.12
T/C mild-notched	0.62	2.05	0.64
T/C sharp-notched	0.52	2.50	1.00
MA unnotched	0.70	1.00	–

support effect, so a consideration of the statistical size effect needs to be included. Hence, the fatigue strength modelling requires also the incorporation of the highly-stressed surface area or volume, which is significantly higher under RB compared to AB loading.

The results under MA loading reveal a decrease of almost 40% compared to the reference value for the unnotched small-scale specimen under T/C loading. This reduction significantly exceeds the evaluated reduction value of about 30% in case of the MA-loaded unnotched small-scale specimen. As the large-scale specimen exhibits a notched geometry and a difference in the highly-stressed surface area or volume, the final fatigue assessment for the multiaxial test condition needs to consider both the micro support and the statistical size effect. Therefore, a validation of the applied fatigue design models for this multiaxial case acts as one major scientific topic of this presented work.

A summary of the fatigue test results for the large-scale specimens is provided in Table 4. Herein again, the statistically evaluated nominal high-cycle fatigue strength as well as the corresponding maximum principal stress concentration factor K_t and normalized relative stress gradient χ' are presented. It has to be pointed out that in case of the MA loading case the numerically evaluated value of K_t is generally dependent on the applied τ/σ-ratio.

Utilizing these evaluated stress conditions and examined differences, a fatigue assessment incorporating the fatigue support as well as the statistical size effect on the basis of highly-stressed surface and volume methods is ensured.

Thereby, the small-scale specimen results in Table 3 act as reference values and the fatigue strength of the large-scale specimen in Table 4 can be estimated, and thus, the validation of theoretical approaches considering both gradient and size effects is possible. With respect to the theoretical modelling of the fatigue strength, the crucial knowledge is also the crack initiation sites and mechanics. Therefore, selected fracture surfaces for AB, RB, and MA loading are shown in Fig. 8. It is clearly observable that crack initiation occurs at the surface in each case. Additionally, this failure mode is found for all tested small and large-scale specimens, see also [52,53]. Especially for surface post-treated components crack initiation may occur beneath the surface [53]. In this case other concepts based on the local fatigue strength distribution in depth, such as presented by [59] for surface-hardened layers, may be more appropriate. However, as the fracture surface analysis in this work reveals a prior surface failure mode, the subsequently utilized fatigue assessment approaches are applicable and a proper practicability is ensured.

Table 4
Summary of fatigue test results for large-scale specimens.

Loading type	Normalized nominal fatigue strength	Stress concentration factor K_t	Normalized relative stress gradient χ'
AB loading	0.94	1.43	0.09
RB loading	0.76	1.43	0.09
MA loading	0.62	2.12	0.07

4. Consideration of micro support effect

This section investigates the applicability of two common stress gradient-based approaches to consider the micro support effect of notched components under fatigue loading. Both methods utilize the fatigue support number n_{SG} to define stress gradient effect. The values of the support number are calculated for both concepts and the values are compared to the uniaxial fatigue test results of the small-scale specimens shown in Table 3. The first applied approach is based on the concept by [33]. It is implemented in the common guideline [22]. Thereby, the evaluation of the fatigue support number $n_{I,SG}$ is presented in Eq. (8) with a reference relative stress gradient of $\chi'_0 = 1\ \mathrm{mm}^{-1}$.

$$n_{I,SG} = 1 + \frac{\chi'}{\chi'_0} \cdot 10^{-\left(a_G - 0.5 + \frac{f_u}{b_G}\right)} \quad \text{for} \quad \chi' < 0.1 \cdot \chi'_0$$
$$n_{I,SG} = 1 + \sqrt{\frac{\chi'}{\chi'_0}} \cdot 10^{-\left(a_G + \frac{f_u}{b_G}\right)} \quad \text{for} \quad 0.1 \cdot \chi'_0 < \chi' < \chi'_0 \tag{8}$$
$$n_{I,SG} = 1 + \sqrt[4]{\frac{\chi'}{\chi'_0}} \cdot 10^{-\left(a_G + \frac{f_u}{b_G}\right)} \quad \text{for} \quad \chi' > \chi'_0$$

The parameters a_G and b_G explain the materials notch sensitivity and they are defined in [22,23]. Thereby, a classification in superior material classes is included, but no further differentiation in sub materials is performed. For steel components the recommendations lie between 0.25 and 0.50 for the factor a_G, and between 2000 and 2700 for b_G. As the investigated steel base material is tested in ESR condition [52], a utilization of the material class considering cast steel may be appropriate, whereby values of $a_G = 0.25$ and $b_G = 2000$ are suggested. However, as the recommendation generally provides parameters for a conservative fatigue assessment, a further adaption of the factors in order to optimize the applicability of the model for 50CrMo4 steel parts in ESR condition may be reasonable.

As introduced, the second approach model $n_{II,SG}$ is presented by [37] and it bases on the evaluated fully reversed fatigue strength under bending $\sigma_{B,R}$ and tension/compression $\sigma_{T/C,R}$ loading, see Eq. (9).

$$n_{II,SG} = 1 + \left(\frac{\sigma_{B,R}}{\sigma_{T/C,R}} - 1\right) \cdot \left(\frac{\chi'}{2/d}\right)^{K_D} \tag{9}$$

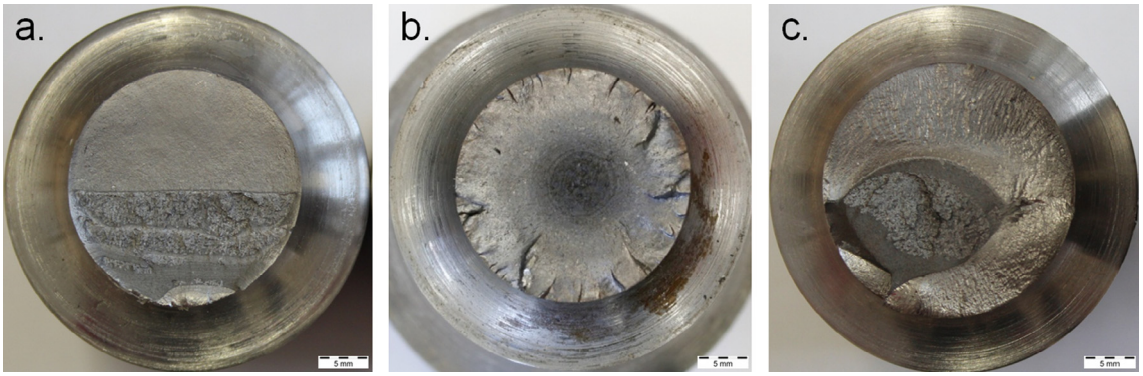

Fig. 8. Fracture surfaces of large-scale specimens tested under AB (a), RB (b), and MA (C) loading.

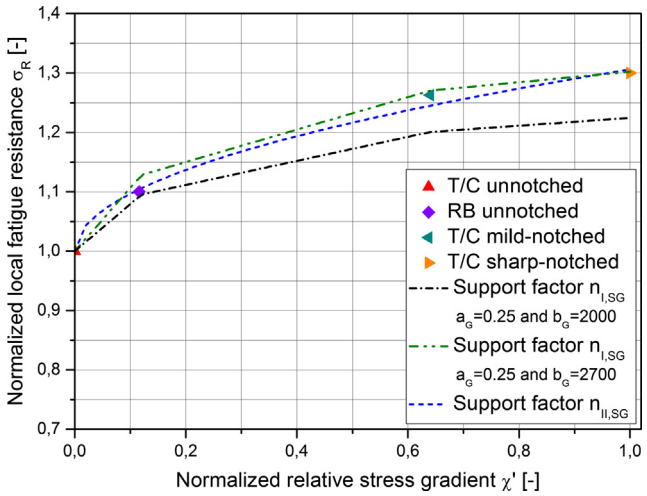

Fig. 9. Comparison of stress gradient based micro support models with fatigue strength of small-scale specimen under uniaxial loading.

In this approach the stress-gradient is related to d equalling the diameter of the unnotched specimens at which the fatigue strength values are experimentally evaluated. Parameter K_D acts as material dependent exponent to define material notch sensitivity. For metallic materials, the parameter K_D usually varies between 0.3 and 0.7 [60]. In [37] a further enhancement of the stress gradient model for the finite life regime in order to ensure a holistically estimation of the local S/N-curve is presented. This procedure is conducted in the course of an interpolation between a minimum and maximum value of the slope in the finite life region k_{min} and k_{max}, and the transition knee point N_{Dmin} and N_{Dmax}. An overview of the approach and a comparison of the stress gradient model to other concepts in literature are provided in [61].

A comparison of the two investigated stress gradient-based micro support models with the experimental results of the uniaxial small-scale specimen fatigue tests is illustrated in Fig. 9. At first, the application of model $n_{I,SG}$ with the recommended parameters for steel castings (black dashed line) reveals a conservative assessment. Especially in case of highly-notched components exhibiting increased relative stress gradients, this approach may lead to a significant oversizing in the course of the design process. As stated, in order to improve the applicability of this model for the investigated steel in ESR condition, an adaption of the incorporated factors may be beneficial. Therefore, just the second parameter b_G is changed to 2700, which is also the suggested value for other steel materials and which distinctively improves the practicability of the model. Hence, the utilization of this second parameter set is suggested in case of 50CrMo4 steel components in ESR condition.

At second, the application of model $n_{II,SG}$ also indicates a sound conformity to the experimentally evaluated fatigue results. A recent study in [62] auxiliary confirms the practicability of the model for a stainless, martensitic steel material. Summarized, both investigated models are well applicable to assess the micro support effect during fatigue loading at notched steel components. However, as fatigue design usually bases on small-scale fatigue test results, the statistical size effect from small to large-scale needs to be additionally taken into account, which is presented in the following part of the paper.

5. Consideration of statistical size effects

This chapter presents the application of two approaches to additionally consider statistical size effects in fatigue analysis. Firstly, the applied models, the highly-stressed surface and volume approach, are shortly explained. Secondly, the computed results are compared with the experimentally evaluated values and discussed in order to present suggestions for the practical fatigue design.

5.1. Surface approach

The first approach bases on the fatigue assessment procedure presented in [43] and incorporated within the guideline given in [22]. The statistical support number $n_{I,ST}$ can be defined by including the ratio of the highly-stressed surface area A_{ref} for a reference specimen and the value A, evaluated for the component, according to Eq. (10).

$$n_{I,ST} = \left(\frac{A_{ref}}{A}\right)^{\frac{1}{k}} \tag{10}$$

The highly-stressed surface area can be evaluated either analytically [63] or numerically, e.g. by the finite element post-processor presented in [64].

In case of complexly-shaped parts the evaluation needs to be performed numerically, but for the investigated large-scale specimen, as representative notched component in this study, an approximation proposed by [63] is available, see Eq. (11). Herein, the constant equals $Y = 2$ for tension, rotating bending and torsion, and $Y = 0.6$ for axial bending loading.

$$A = Y \cdot \pi \cdot \frac{d}{2} \cdot \frac{R}{2} \tag{11}$$

As comprehensive numerical analysis results of the large-scale specimen are available, an evaluation based on the finite element output data is comparably performed. Based on [22], the reference surface A_{ref} should be defined as 500 mm^3 as this equals the value for the small-scale material specimens within the guideline. However, in this paper own small-scale specimen results act as fundament for the fatigue assessment and therefore, also the reference values for these geometries need to be incorporated. An analytical evaluation of the unnotched small-scale specimen geometry under tension/compression loading, which is presented in [52], leads to a reference surface area of $A_{ref} = 589$ mm^3. Besides the highly-stressed surface area, also the Weibull exponent k needs to be defined for the assessment of the statistical size-effect. According to [43], this parameter exhibits a value of $k = 15$ for the selected material class, which is used within the fatigue assessment in this work.

Local stress-based fatigue approaches generally utilize linear-elastic material behaviour in order to compute the notch stress state. As an increased stress concentration at the notch region may lead to local plastic deformation during fatigue loading, the approximation formulae according to [65] is applied to correlate the hypothetical linear-elastic state σ_{el} and ε_{el} with the real local stress σ and strain ε condition, see Eq. (12).

$$\sigma \cdot \varepsilon = \sigma_{el} \cdot \varepsilon_{el} = \frac{\sigma_{el}^2}{E} \tag{12}$$

Furthermore, the local strain ε_R at the high-cycle fatigue strength level $\sigma_{T/C,R}$ can be separated into an elastic $\varepsilon_{el,R}$ and plastic part $\varepsilon_{pl,R}$ according to Eq. (13).

$$\varepsilon_R = \varepsilon_{el,R} + \varepsilon_{pl,R} = \frac{\sigma_{T/C,R}}{E} + \varepsilon_{pl,R} \tag{13}$$

Finally, the macro fatigue support effect number $n_{I,MS}$ can be defined as shown in Eq. (14). As the size of the highly-stressed area influences this factor, the statistical size effect is additionally considered on the basis of the previously defined support number $n_{I,ST}$. Values for plastic strain amplitudes $\varepsilon_{pl,R}$ of steel materials in the high-cycle fatigue region as well as recommendations for the exponent n' can be derived from [66].

$$n_{I,MS} = \sqrt{1 + \frac{E \cdot \varepsilon_{pl,R}}{\sigma_{T/C,R}} \cdot n_{I,ST}^{\frac{1}{\psi}-1}} \tag{14}$$

utilizing the following values for the investigated 50CrMo4 steel ($f_u > f_{u,ref}$ = 630 MPa)

$$\varepsilon_{pl,R} = 2 \cdot 10^{-4} \cdot \psi \quad \text{with} \quad \psi = 1 - 0.375 \cdot \left(\frac{f_u}{f_{u,ref}} - 1\right)$$

In order to incorporate not only statistical and fatigue support effects, an enhancement of the assessment procedure by the geometrical size effect is presented in [43]. Thereby, a fracture mechanical support number $n_{I,FM}$ is defined, which bases on the short-crack growth approach considering the suggested model by [67,68], see Eq. (15).

$$n_{I,FM} = \frac{K_t}{n_{I,ST} \cdot n_{I,MS} + \sqrt{\frac{\hat{a}}{a^*}}} \tag{15}$$

Herein, the material parameter a^* serves as characteristic defect or respectively crack length under which a certain crack free high-cycle fatigue strength is applicable. In case of multiaxial loading, the stress concentration factor K_t needs to be considered separately for each uniaxial loading type, see [22]. Above this value an increase of the defect size or crack length leads to a decrease of the fatigue strength. The parameter a^* is usually determined on the basis of the threshold value in the long-crack regime, however, a review of material data in [43] proposes the approximation formula according to Eq. (16).

$$a^* = a_0^* \cdot \left(\frac{f_u^*}{f_u}\right)^2 \tag{16}$$

Herein, the factor a_0^* is defined as 0.1 mm and f_u^* as 680 MPa for steel [43]. An estimation with an ultimate strength of f_u = 1000 MPa for the investigated steel reveals a characteristic crack length of a^* = 46.2 μm. Although the base material is tested in ESR condition, previously conducted microscopical analyses in [52] indicate an average maximum inclusion size of 5.2 ± 1.1 μm. However, as this value is significantly beneath the estimated characteristic length a^*, a certain influence by the inclusions on the fatigue assessment model is basically not assumed. Hence, the presented approach considering the fracture mechanical based support number $n_{I,FM}$ is well utilizable for the investigated base material.

The second parameter $\hat{a}$ incorporates the relative stress gradient χ' as well as the stress concentration factor K_t at the surface of the notch root, see Eq. (17). Further formulae for the assessment of complexly-shaped components without the need to define a nominal cross-section and to calculate K_t is given in [43].

$$\hat{a} = \frac{1}{\chi'} \cdot \frac{(2 \cdot K_t + 1) \cdot (K_t - 1)^2}{4 \cdot K_t} \tag{17}$$

Summarized, the final support number n_I of the first surface based approach is calculated by multiplying the statistical $n_{I,ST}$, macro fatigue support $n_{I,MS}$, and fracture mechanical support number $n_{I,FM}$ as illustrated in Eq. (18). As introduced, the local fatigue strength $\sigma_{R,I}$ is finally evaluated as shown in Eq. (19).

$$n_I = n_{I,ST} \cdot n_{I,MS} \cdot n_{I,FM} \tag{18}$$

$$\sigma_{R,I} = \sigma_{T/C,R} \cdot n_I \tag{19}$$

5.2. Volume approach

The second approach is presented in [46] and acts as enhancement of the stress gradient concept by [37]. This model utilizes the highly-stressed volume V as relevant parameter to assess the statistical support number $n_{II,ST}$ and again bases on the Weibull's theory in [40] incorporating a material dependent exponent a, see Eq. (20).

$$n_{II,ST} = \left(\frac{V}{V_{ref}}\right)^a \tag{20}$$

The parameter a can be derived by experimental evaluation of the high-cycle fatigue strength under AB and RB loading, denoted as $\sigma_{AB,R}$ and $\sigma_{RB,R}$, and its corresponding values for the highly-stressed material volume, denoted as V_{AB} and V_{RB}, according to Eq. (21).

$$a = \log\left(\frac{\sigma_{AB,R} \cdot V_{RB}}{\sigma_{RB,R} \cdot V_{AB}}\right) \tag{21}$$

In [69] it is suggested to define the highly-stressed volume by a decrease down to 90% of the peak stress value within the evaluated region, which is also applied in this work. A study in [46] for various engineering materials reveals that for steel the parameter a exhibits value of around 0.96. However, a detailed computation of this value on the basis of the presented fatigue test results in this work is presented in the next section. In the course of the application of this model, firstly, the presented stress gradient approach by [37] is enhanced by the highly-stressed volumes of the investigated small-scale specimens under T/C and RB loading, namely $V_{T/C}$ and V_{RB}, leading to a corrected support number $n_{II,SG,corr}$, see Eq. (22).

$$n_{II,SG,corr} = \left(1 + \left(\frac{\sigma_{RB,R}}{\sigma_{T/C,R}} \cdot \left(\frac{V_{RB}}{V_{T/C}}\right)^a - 1\right) \cdot \left(\frac{\chi'}{2/d}\right)^{K_D}\right) \tag{22}$$

A graphical representation of the numerically evaluated highly-stressed volumes of the unnotched small-scale specimens under T/C and RB loading are depicted in Figs. 10 and 11. The results reveal that in case of RB loading the highly-stressed volume is localized on a comparably small, surface-near material layer leading to a minor value of only V_{RB} = 47 mm^3. This condition is significantly smaller compared to the behaviour under T/C loading with $V_{T/C}$ = 376 mm^3, whereby the whole cross-section is highly-stressed.

Secondly, the consideration of the statistical size effect occurring from the small-scale specimen to the large-scale component is incorporated on the basis of Eq. (23).

$$n_{II} = \left(1 + \left(\frac{\sigma_{RB,R}}{\sigma_{T/C,R}} \cdot \left(\frac{V_{RB}}{V_{T/C}}\right)^a - 1\right) \cdot \left(\frac{\chi'}{2/d}\right)^{K_D}\right) \cdot \left(\frac{V_{T/C}}{V}\right)^a \tag{23}$$

Herein, the highly-stressed volume of the component V is additionally considered, which enables a combined fatigue assessment involving both the micro support effect based on the stress gradient as well as the statistical size effect. Finally, the calculation of the local high-cycle fatigue strength $\sigma_{R,II}$ again utilizes the fatigue resistance under T/C loading $\sigma_{T/C,R}$ multiplied by the fatigue support number n_{II}, see Eq. (24).

$$\sigma_{R,II} = \sigma_{T/C,R} \cdot n_{II} \tag{24}$$

In the following section, the high-cycle fatigue strengths based on the surface and volume approach, denoted as $\sigma_{R,I}$ and $\sigma_{R,II}$, are evaluated for the large-scale specimens, as representative notched steel component, within this study. In addition, a validation of the assessed values with the experimental results and a final discussion to highlight certain benefits and drawbacks of each method are provided.

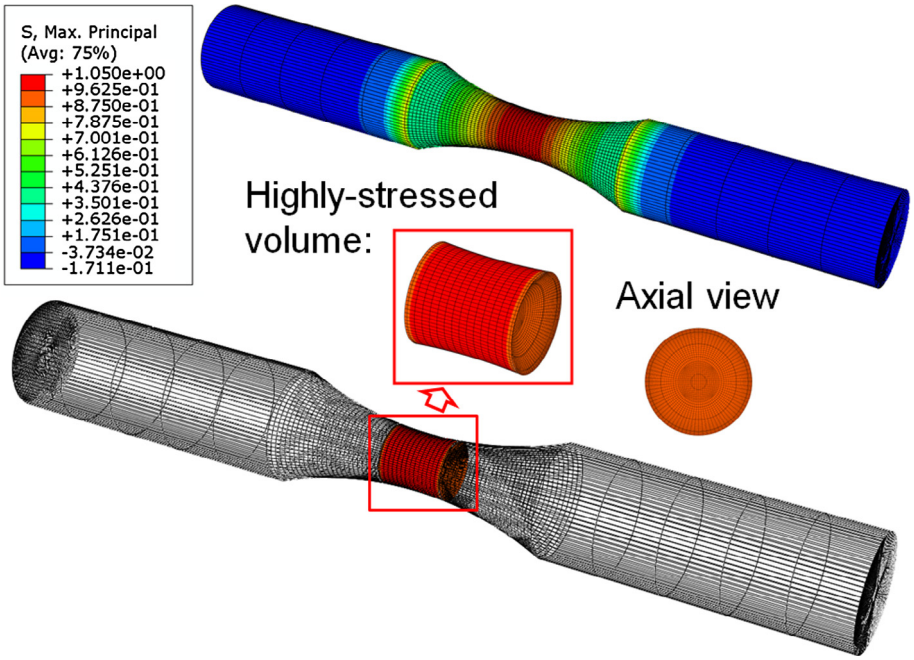

Fig. 10. Numerical evaluation of highly-stressed volume ($V_{T/C}$ = 376 mm^3) for unnotched small-scale specimen under tension/compression (T/C) loading.

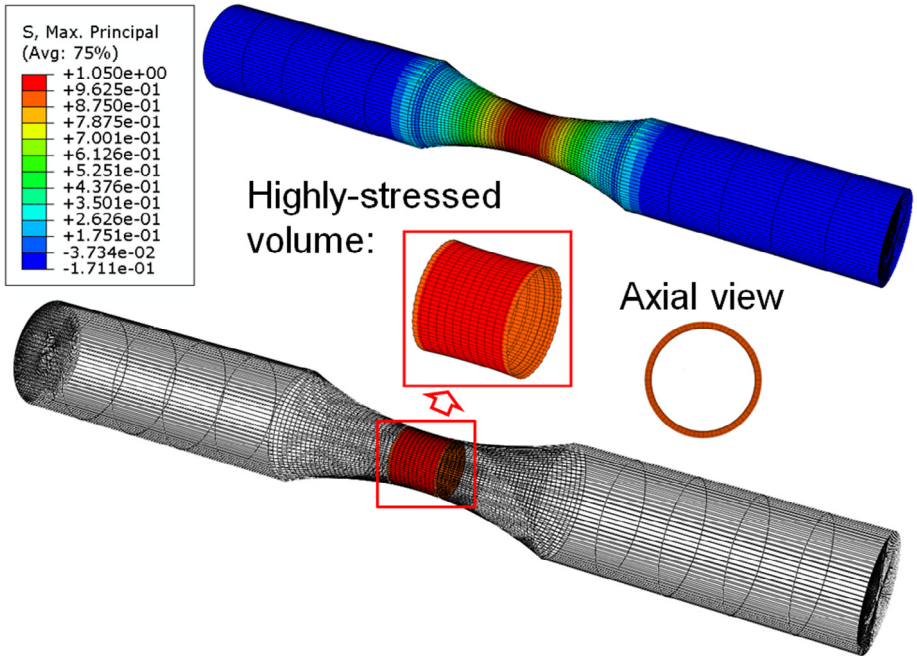

Fig. 11. Numerical evaluation of highly-stressed volume (V_{RB} = 47 mm^3) for unnotched small-scale specimen under rotating bending (RB) loading.

5.3. Discussion of the results

Based on the presented linear-elastic numerical analysis of the large-scale specimens under the investigated loading types, an evaluation of the highly-stressed surface area and volume is conducted. The resulting highly-stressed surface area A for the large-scale specimen under AB loading is illustrated in Fig. 12a. Furthermore, a representation of the three-dimensional stress distribution for the evaluation of the highly-stressed volume is depicted by a three-quarter model view in Fig. 12b. As aforementioned, in accordance to a suggestion by [69], stress values within 90% of the evaluated peak stress are considered in both cases.

In case of the surface approach, a comparison of the numerically evaluated highly-stressed surface areas with the presented analytical approximation formula in [63] is enabled. Thereby, an average value of Y = 1.3 is applied for MA loading to cover both torsion and axial bending. The results utilizing the analytical procedure indicate a minor overestimation up to only 4% compared to the numerical assessment for the large-scale specimen.

These findings validate the applicability of the suggested formula in [63], however, for complexly-shaped components, a numerical analysis is still necessary as no general approximation formulae for multiaxial stress states are provided. A summary of the values for the highly-stressed surface area and volume for

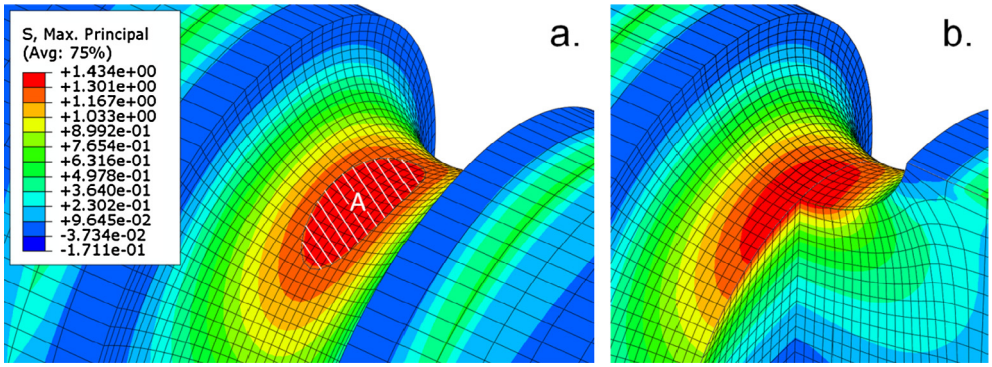

Fig. 12. Highly-stressed surface area A (a) and three-dimensional stress distribution for evaluation of highly-stressed volume (b) for large-scale specimen AB loading.

Table 5
Evaluated highly-stressed surface and volume values for large-scale specimens.

Loading type	Highly-stressed area A [mm^2]	Highly-stressed volume V [mm^3]
AB loading	60	68
RB loading	401	480
MA loading	260	231

the large-scale specimens is shown in Table 5. A calculation of a nominal highly-stressed layer thickness as ratio of the volume to the surface area reveals a value of 1.1 mm for AB, 1.2 mm for RB, and 0.9 mm for MA loading. Hence, the evaluated highly-stressed volume seems to be specifically localized in the surface-layer, which is also validated by the detected crack initiation in this area in the course of the fracture surface analysis of the tested specimens.

In order to apply the surface and volume approach, the exponent k and a need to be evaluated for the investigated 50CrMo4 steel material. As previously described, this can be performed by utilizing the high-cycle fatigue strength values of the large-scale specimens under AB and RB loading and the corresponded values of the highly-stressed surface area and volume. Regarding the surface approach, an exponent of $k = 15$, which is recommended for steel castings in [43], is well applicable and leads to conservative assessment with an underestimation of the fatigue strength by only 2.6%. Focussing on the volume approach, an exponent of $a = 0.94$ is empirically determined, which fits quite well to the previously published values for steel materials in [46].

A comparison of the evaluated nominal high-cycle fatigue strength results of the large-scale specimen by the experiments and the surface approach is shown in Table 6. Thereby, this first method based on the highly-stressed surface leads to a sound accordance to the fatigue tests. For each loading condition, fatigue strength is slightly underestimated having a maximum conservative deviation of 7.4% for AB loading. Differences, which are exclusively caused by the statistical size effect, are generally taken quite well into account by comparing the fatigue strength results under AB and RB loading. Additionally, this procedure is also well applicable for the investigated MA load scenario with a minor underestimation of the fatigue strength by only 3.2%. Summarized, the surface approach shows a feasible practicability for both uniaxial and multiaxial loadings and the estimated results fit well to the fatigue tests.

On the contrary, the volume approach reveals some limitations in the course of the application. According to [70], an upper highly-stressed volume limit for the utilization of the method exists, which is estimated to be a value of about $V = 50$ mm^3 for forged steel. However, for the large-scale specimen in this work it reveals that this threshold value may be set to $V = 80$ mm^3 for the incorporated uniaxial and $V = 60$ mm^3 for the considered multiaxial stress state. Hence, in case of AB loading, the numerically evaluated highly-stressed volume of $V = 68$ mm^3 is applicable, but for RB and MA loading the presented upper limits of $V = 80$ mm^3 and $V = 60$ mm^3 need to be taken as basis for the assessment in order to avoid a major underestimation of the fatigue strength.

Therefore, these highly-stressed upper limit volumes are considered for the final fatigue assessment. The results are compared to the experiments in Table 6, again as normalized values with respect to the high-cycle fatigue resistance of the unnotched small-scale specimen under T/C loading. It is shown that the volume approach also leads to a sound conformity with the fatigue test results exhibiting a maximum deviation of only 4.3% if the evaluated upper threshold values are maintained. For comparison, a utilization of the numerically evaluated volumes in Table 5, which exceed the threshold volume, would lead to a fatigue strength underestimation by about 80% in case of RB and by roughly 70% for MA loading. Hence, the definition of a certain upper threshold volume, as suggested in [70], is of great importance in order to ensure a proper fatigue design.

To summarize, both analyzed approaches reveal a well practicability for the investigated 50CrMo4 large-scale steel specimens as representative component for design. However, in the course of the application is it shown that for the volume approach a certain material and loading dependent upper threshold value of the highly-stressed volume needs to be defined. This fact may be considered as drawback of this method as for the surface approach such a definition is not specifically needed. On the one hand, the highly-stressed surface concept may be favourable in case of mate-

Table 6
Comparison of nominal fatigue strength values for large-scale specimen by experiments and fatigue assessment models.

Loading type	Normalized nominal fatigue strength by fatigue testing	Normalized nominal fatigue strength by surface approach $\sigma_{R,I}$	Normalized nominal fatigue strength by volume approach $\sigma_{R,II}$
AB loading	0.94	0.87 (−7.4%)	0.90 (−4.3%)
RB loading	0.76	0.74 (−2.6%)	0.77 (+1.3%)
MA loading	0.62	0.60 (−3.2%)	0.64 (+3.2%)

rials exhibiting less volume imperfections presumably leading to a crack initiation at the surface. On the other hand, for defective materials, e.g. casted materials including shrinkage or gas pores, the application of the volume approach may feature advantages as not only the surface, but additionally the influence of the flawed material volume is incorporated. For a proper feasibility, the upper threshold volumes need to be defined empirically, whereby influences by the loading mode as well as local material characteristics, such as the inclusion size distribution or the microstructure based on grain size and orientation, may occur. Such effects are also observed in this work, as the assessed upper limit volume shows a difference between the uniaxial and multiaxial loading condition. Concluding, for prior surface failure modes the presented surface approach is preferable due its engineering feasible applicability. In case of subsurface crack initiation, which may occur due to inhomogeneities, such as inclusions or defects within the material, the volume approach may be more appropriate, whereby special attention in regard to properly estimate the material and loading dependent upper threshold volume needs to be taken.

6. Conclusions

This paper investigates the fatigue support and statistical size effect of notched 50CrMo4 steel components under uniaxial and multiaxial proportional loading conditions. Based on the presented experimental and numerical analyzes for the incorporated small and large-scale specimens, the following conclusions can be drawn:

- The common stress gradient models by [33], as incorporated in [22,37] are well suitable for fatigue assessment of notched electroslag remelted steel components.
- Linear-elastic numerical analyses of the large-scale specimen, as representative notched component, reveals that the suggested analytical approximation formula in [63] is well applicable and leads to a minor overestimation of the highly-stressed surface area by only 4% compared to the numerical results. The numerically computed highly-stressed volumes show a distinctive localization at the surface-layer under all considered load conditions. An estimation of a nominal highly-stressed layer thickness reveals an average value of about 1 mm, which is also validated by the fracture surface analysis indicating a favourable crack origin from the surface for almost all tested specimens.
- An application of a surface [43] and volume based [46] approach considering both fatigue support and statistical size effects is presented for the large-scale specimen. Firstly, the assessed high-cycle fatigue strength by the surface approach shows sound conformity with the experiments exhibiting a minor maximum deviation of only 7.4% in case of AB loading. In addition, the concept is well practicable for the investigated MA load condition, whereby a comparably small underestimation by only 3.2% is observed. Secondly, the volume approach shows some drawbacks in regard to a certain upper threshold limit of the highly-stressed volume as shown in [69]. A study for the investigated 50CrMo4 steel illustrates that these upper limits may be set to $V = 80\ mm^3$ for the incorporated uniaxial and $V = 60\ mm^3$ for the considered multiaxial stress state. Utilizing these values, again a sound agreement between the assessed high-cycle fatigue strength values and the experimental results is achieved with a maximum deviation of only 4.3%.

In conclusion, the surface approach may be preferably applied in case of preferential occurrence of surface failure modes, as shown for the large-scale specimens within this study. On the contrary, the volume approach may be advantageous for subsurface crack initiation, which may arise for inclusion-afflicted material [71] or components with post-treated surface-layers [72]. However, in this case an applicable upper threshold limit of the highly-stressed volume needs to be defined in order to ensure a proper fatigue assessment.

A further scheduled working topic deals with the size effect of surface-treated components. Mechanical post-treatment or hardening processes majorly affect the surface material layer of components and its fatigue performance. In order to optimize the fatigue life, the relationship between the hardened surface-layer and the component size as well as the loading condition is of utmost importance. Therefore, additional size effects occur, which may influence the definition of specific process parameters within the post-treatment [73]. A final consideration of the manufacturing process and fatigue loading dependent characteristics, like variable load amplitudes or multiaxiality [74], on the fatigue life of complexly-shaped components exhibiting different sizes is defined as goal for the prospective scientific work.

References

[1] Savaidis G, Savaidis A, Tsamasphyros G, Zhang C. On size and technological effects in fatigue analysis and prediction of engineering materials and components. Int J Mech Sci 2002;44:521–43.
[2] Furuya Y. Notable size effects on very high cycle fatigue properties of high-strength steel. Mater Sci Eng, A 2011;528:5234–40.
[3] Shirani M, Härkegård G. Fatigue life distribution and size effect in ductile cast iron for wind turbine components. Eng Fail Anal 2011;18:12–24.
[4] Tomaszewski T, Sempruch J, Piątkowski T. Verification of selected models of the size effect based on high-cycle fatigue testing on mini specimens made of EN AW-6063 aluminum alloy. J Theor Appl Mech 2014;52:883–94.
[5] Wang GY, Liaw PK, Yokoyama Y, Inoue A. Size effects on the fatigue behavior of bulk metallic glasses. J Appl Phys 2011;110:113507.
[6] Klein M, Hadrboletz A, Weiss B, Khatibi G. The 'size effect' on the stress–strain, fatigue and fracture properties of thin metallic foils. Mater Sci Eng, A 2001;319–321:924–8.
[7] Kaffenberger M, Vormwald M. Considering size effects in the notch stress concept for fatigue assessment of welded joints. Comput Mater Sci 2012;64:71–8.
[8] Sosnovskii LÀ, Zhmailik VÀ, Komissarov VV. Size effect in contact fatigue. Strength Mater 2009;41:88–94.
[9] Dini D, Nowell D, Korsunsky AM. Size and scale effects in fretting fatigue thresholds. Int J Fract 2005;135:L11–8.
[10] Kloos KH. Einfluß des Oberflächenzustands und der Probengröße auf die Schwingfestigkeitseigenschaften. VDI-Report, vol. 268; 1976. p. 63–76.
[11] Makkonen M. Statistical size effect in the fatigue limit of steel. Int J Fatigue 2001;23:395–402.
[12] Bazios I, Gudladt H-J. The fatigue lifetime estimation in consideration of the statistical size effect as example for the AlMgSi0.7 alloy. Mat-wiss u Werkstofftech 2004;35:21–8 [in German].
[13] Kreuzer W, Heckel K. Prediction of the fatigue strength of welded joints based on the statistical size effect. Mat-wiss u Werkstofftech 1999;30:87–94 [in German].
[14] Kloos KH, Buch A, Zankov D. Pure geometrical size effect in fatigue tests with constant stress amplitude and in programme tests. Z Werkstofftech 1981;12:40–50 [in German].
[15] Cova M, Nanni M, Tovo R. Geometrical size effect in high cycle fatigue strength of heavy-walled ductile cast iron GJS400: weakest link vs defect-based approach. Proc Eng 2014;74:101–4.
[16] Taylor D. Geometrical effects in fatigue: a unifying theoretical model. Int J Fatigue 1999;21:413–20.
[17] Shirani M, Härkegård G. Large scale axial fatigue testing of ductile cast iron for heavy section wind turbine components. Eng Fail Anal 2011;18:1496–510.
[18] Kainzinger P, Grün F. Mean stress sensitivity of ductile iron with respect to technological and statistical size effect considering defects. In: MATEC web of conferences, vol. 12; 2014. p. 03004.
[19] Zamiri F, Acevdo C, Nussbaumer A, Krummenacker J. Investigation of technological size effects of welding on the residual stresses and fatigue life of tubular joints made of structural steels S355 and S690. In: Proceedings of fatigue design conference; 2011.
[20] Pavlov VF, Kirpichev VA, Vakulyuk VS, Sazanov VP. Surface hardening influence on the fatigue limit for cylindrical parts of different diameter. Russian Aeronaut 2013;57:324–6.
[21] Liu J, Zenner H. Fatigue limit and geometrical and statistical size effect. Mat-wiss u Werkstofftech 1991;22:187–96 [in German].
[22] FKM-Guideline: Analytical Strength Assessment of Components in Mechanical Engineering, 6th revised edition, VDMA, Frankfurt; 2012.

[23] McKelvey SA, Lee Y-L, Barkey ME. Stress-based uniaxial fatigue analysis using methods described in FKM-guideline. J Fail Anal Prev 2012;12:445–84.
[24] Radaj D. Review of fatigue strength assessment of nonwelded and welded structures based on local parameters. Int J Fatigue 1996;18:153–70.
[25] Niessner M, Seeger T, Hohe J, Siegele D. Strength calculation of sharp notched components. Mat-wiss u Werkstofftech 2003;34:797–811 [in German].
[26] Zhang G. Method of effective stress for fatigue: Part I – a general theory. Int J Fatigue 2012;37:17–23.
[27] Neuber H. Über die Berücksichtigung der Spannungskonzentration bei Festigkeitsberechnungen (On the allowance of stress concentrations in strength calculations). Konstruktion 1968;20(7):245–51 [in German].
[28] Radaj D, Lazzarin P, Berto F. Generalised Neuber concept of fictitious notch rounding. Int J Fatigue 2013;51:105–15.
[29] Creager M, Paris PC. Elastic field equations for blunt cracks with reference to stress corrosion cracking. Int J Fract Mech 1967;3:247–52.
[30] Peterson RE. Notch sensitivity. Metal fatigue, New York: MacGraw-Hill; 1959. p. 293–306.
[31] Heywood RE. Designing against fatigue. London: Chapman and Hall; 1962.
[32] Ciavarella M, Meneghetti G. On fatigue limit in the presence of notches: classical vs. recent unified formulations. Int J Fatigue 2004;26:289–98.
[33] Siebel E, Stieler M. Ungleichförmige Spannungsverteilung bei schwingender Beanspruchung (Irregular stress distribution at cyclic loading), VDI Veröffentlichung 97; 1955 [in German].
[34] Spaggiari A, Castagnetti D, Dragoni E, Bulleri S. Fatigue life prediction of notched components: a comparison between the theory of critical distance and the classical stress-gradient approach. Proc Eng 2011;10:2755–67.
[35] VDI-Richtlinie 2226: Recommendation for the stability calculation of metallic building components, VDI-Verlag, Düsseldorf; 1965 [in German].
[36] Hück H, Thrainer L, Schütz W. Berechnung von Wöhlerlinien für Bauteile aus Stahl, Stahlguss und Grauguss: Synthetische Wöhlerlinien (Calculation of Wöhler curves for components made of steel, steel casting and gray cast iron), Bericht Nr. ABF 11, VDEh, Düsseldorf; 1981 [in German].
[37] Eichlseder W. Fatigue analysis by local stress concept based on finite element results. Comput Struct 2002;80:2109–13.
[38] Gaier C, Dannbauer H. Fatigue analysis of multiaxially loaded components with the FE-postprocessor FEMFAT-MAX. Eur Struct Integrity Soc 2003;31:223–40.
[39] Flaceliere L, Morel F. Probabilistic approach in high-cycle multiaxial fatigue: volume and surface effects. Fatigue Fract Eng Mater Struct 2004;27:1123–35.
[40] Weibull W. A statistical theory of the strength of materials. Royal Swed Inst Eng Res 1939;151.
[41] Friederich H, Kaiser B, Kloos KH. Anwendung der Fehlstellentheorie nach Weibull zur Berechnung des statistischen Größeneinflusses bei Dauerschwingbeanspruchung (Application of defect theory according to Weibull to assess the statistical size effect at cyclic loading). Mat-wiss u Werkstofftech 1998;29:178–84 [in German].
[42] Heckel K, Köhler J. Experimental investigation of the statistical size-effect in fatigue tests with unnotched specimens. Z Werkstofftech 1975;2: 52–54 [in German].
[43] Hertel O, Vormwald M. Statistical and geometrical size effects in notched members based on weakest-link and short-crack modelling. Eng Fract Mech 2012;95:72–83.
[44] Norberg S, Olsson M. The effect of loaded volume and stress gradient on the fatigue limit. Int J Fatigue 2007;29:2259–72.
[45] Van Hooreweder B, Moens D, Boonen R, Sas P. Fatigue strength analysis of notched aluminium specimens using the highly stressed volume method. Fatigue Fract Eng Mater Struct 2011;35:154–9.
[46] Fröschl J, Decker M, Eichlseder W. A new approach for consideration of stress-mechanical and statistical size effect. Mater Test 2011;53:481–6 [in German].
[47] Gänser H-P. Some notes on gradient, volumetric and weakest link concepts in fatigue. Comput Mater Sci 2008;44:230–9.
[48] Krä C, Heckel K. Transfer of fatigue life data with the statistical size effect. Mat-wiss u Werkstofftech 1989;20:255–61 [in German].
[49] Palin-Luc T. Stress gradient and size effects in multiaxial fatigue. Munich/Germany: Materials Week; 2000.
[50] Gates N, Fatemi A. Notch deformation and stress gradient effects in multiaxial fatigue. Theoret Appl Fract Mech 2016;84:3–25.
[51] Luu DH, Maitournam MH, Nguyen QS. Formulation of gradient multiaxial fatigue criteria. Int J Fatigue 2014;61:170–83.
[52] Leitner M, Tuncali Z, Steiner R, Grün F. Multiaxial fatigue strength assessment of electroslag remelted 50CrMo4 steel crankshafts. Int J Fatigue 2017;100:159–75.
[53] Leitner M, Tuncali Z, Chen W, Grün F. Mechanical post-treatment of induction-hardened surface layers to optimize fatigue strength of crankshafts. In: Materials science and engineering conference, Darmstadt/Germany; 2016.
[54] Steels for quenching and tempering – Part 3: Technical delivery conditions for alloy steels English version of DIN EN 10083-3:2007-01; 2007.
[55] Schuscha M. Test rig design to characterize fatigue strength under multiaxial stress states. Master thesis. Montanuniversität Leoben; 2016 [in German].
[56] ASTM E739: Standard practice for statistical analysis of linear or linearized stress-life (S-N) and strain-life (e-N) fatigue data; 1998.
[57] Dengel D. Arc sine$\sqrt{P}$-transformation – an effective tool for graphical and numerical evaluation of planned Wöhler-experiments. J Mater Technol 1975;8:253–61.
[58] Gough HJ, Pollard HV, Clenshaw WJ. Some experiments on the resistance of metals under combined stress, Aeronautical Research Council, 2522. London: His Majesty's Stationary Office; 1951.
[59] Kloos KH, Velten E. Berechnung der Dauerschwingfestigkeit von plasmanitrierten bauteilähnlichen Proben unter Berücksichtigung des Härte- und Eigenspannungsverlaufes (Calculation of endurance limit of plasma-nitrated component-related specimens considering hardness and residual stress distribution). Konstruktion 1984;36:181–8.
[60] Eichlseder W. Fatigue life prediction based on finite element results. Mat-wiss u Werkstofftech 2003;34:843–9 [in German].
[61] Eichlseder W, Leitner H. Influence of stress gradient on S/N-curve, proceedings of the conference new trends in fatigue and fracture, Metz/France; 2002.
[62] Milošević I, Winter G, Grün F, Kober M. Influence of size effect and stress gradient on the high-cycle fatigue strength of a 1.4542 steel. Proc Eng 2016;160:61–8.
[63] Liu J. Dauerfestigkeitsberechnung metallischer Bauteile (Assessment of endurance limit of metallic components), TU Clausthal; 2001 [in German].
[64] Diemar A, Thumser R, Bergmann J. Statistischer Größeneinfluss und Bauteilfestigkeit (Statistical size effect and component size), MP Materialprüfung 2004;46: 16–21 [in German].
[65] Neuber H. Theory of stress concentration for shear-strained prismatical bodies with arbitrary nonlinear stress–strain law. Trans ASME, J Appl Mech 1961;28:544–50.
[66] Bäumel A, Seeger T. Materials data for cyclic loading. Amsterdam: Elsevier Science Publishers; 1990.
[67] El Haddad MH, Topper TH, Smith KN. Prediction of non propagating cracks. Eng Fract Mech 1979;11:573–84.
[68] Kitagawa H, Takahashi S. Applicability of fracture mechanics to very small cracks or the cracks in the early stage. In: 2nd int conf on mechanical behavior of materials, Boston/USA; 1976. p. 627–31.
[69] Sonsino CM. Zur Bewertung des Schwingfestigkeitsverhaltens von Bauteilen mit Hilfe örtlicher Beanspruchungen (Assessment of fatigue strength behaviour of components by means of local stresses). Konstruktion 1993;45:25–33 [in German].
[70] Kaufmann H. Zur schwingfesten Bemessung dickwandiger Bauteile aus GGG-40 unter Berücksichtigung gießtechnisch bedingter Gefügeungänzen (Fatigue assessment of GGG-40 components considering casting-related microstructural discontinuities), Dissertation. Technische Fakultät der Universität Saarland; 1998 [in German].
[71] Wang QY, Bathias C, Kawagoishi N, Chen Q. Effect of inclusion on subsurface crack initiation and gigacycle fatigue strength. Int J Fatigue 2002;24:1269–74.
[72] Tjernberg A. Fatigue lives for induction hardened shafts with subsurface crack initiation. Eng Fail Anal 2002;9:45–61.
[73] Kloos KH. Size effect and fatigue properties with respect to optimized surface-treatment. Z Werkstofftech 1981;12:134–42 [in German].
[74] Vormwald M. Multi-challenge aspects in fatigue due to the combined occurrence of multiaxiality, variable amplitude loading, and size effects. Frattura ed Integrità Strutturale 2015;33:253–61.